sustainability

MDPI

Article

Thiocracking of Multi-Materials: High-Strength Composites from Post-Consumer Food Packaging Jars

Katelyn M. Derr and Rhett C. Smith *

Department of Chemistry, Clemson University, Clemson, SC 29634, USA
* Correspondence: rhett@clemson.edu

Abstract: A significant waste material threatening sustainability efforts are post-consumer food packaging goods. These ubiquitous multi-materials comprise chemically disparate components and are thus challenging targets for recycling. Herein, we undertake a proof-of-principle study in which we use a single-stage method to convert post-consumer multi-material food packaging (post-consumer peanut butter jars) to a high compressive strength composite ($PBJS_{90}$). This is accomplished by thiocracking the ground jar pulp (10 wt. %) with elemental sulfur (90 wt. %) at 320 °C for 2 h. This is the first application of thiocracking to such mixed-material post-consumer goods. Composite synthesis proceeded with 100% atom economy, a low E factor of 0.02, and negative global warming potential of −0.099 kg CO_2e/kg. Furthermore, the compressive strength of $PBJS_{90}$ (37.7 MPa) is over twice that required for Portland cement building foundations. The simplicity of composite synthesis using a lower temperature/shorter heating time than needed for mineral cements, and exclusive use of waste materials as precursors are ecologically beneficial and represent an important proof-of-principle approach to using thiocracking as a strategy for upcycling multi-materials to useful composites.

Keywords: chemical recycling; multi-materials; packaging; PET; thiocracking; sulfur

Citation: Derr, K.M.; Smith, R.C. Thiocracking of Multi-Materials: High-Strength Composites from Post-Consumer Food Packaging Jars. *Sustainability* **2024**, *16*, 7023. https://doi.org/10.3390/su16167023

Academic Editor: Giulio Mario Cappelletti

Received: 25 June 2024
Revised: 30 July 2024
Accepted: 12 August 2024
Published: 16 August 2024

1. Introduction

Despite strides in chemical recycling methods for various types of plastics, the quantity of plastic waste deposited in landfills or incinerated far exceeds the quantity recycled [1,2]. The amount of landfilled plastic waste is projected to grow at an exponentially faster rate than its recycling and incineration [3–5], and it is already estimated that 91% of plastic waste is deposited as litter in the environment or landfilled, rather than recycled [6–9]. Plastics exposed to the elements in the environment can shed microplastics, fibers, and other pollutants into the atmosphere, water systems, and surrounding areas, leading to detrimental effects on the environment, ecological systems, and human health [10–22]. There is a dire need to ameliorate these detrimental effects by finding improved methods for chemically recycling various plastics [23–41]. Many single-use packaging items in circulation today are multi-materials comprised of various plastics, paper, and other materials, often in multi-layer assemblies fixed together by adhesives that are not easy to physically separate into their chemically distinct components [42–47]. Familiar examples include plastic jars or bottles having paper or plastic labels. The separation process is further complicated in many cases by contamination of packaging components with unused goods such as food waste in discarded jars and bottles. Mixed-composition waste thus poses a colossal challenge for chemical recycling, in particular due to the divergent chemical reactivity of each component. In order to create a quintessential green economy, it is necessary to design recycling methods that can address various plastics and materials in a single process. Thiocracking is a promising approach in this regard. Thiocracking is a general term for the breakdown of organic polymeric materials by heating them in the presence of elemental sulfur [48–51]. Because elemental sulfur is a byproduct of the oil refining process stockpiled at waste sites [52,53], its utilization further contributes positively to sustainability and environmental remediation goals [54–122]. Thiocracking has proven effective in chemical recycling/upcycling of a wide range of synthetic plastics and biopolymers including polyesters [49,123–125], polyacrylics [50], polycarbonates [51], lignin [126–128], cellulose [129], starch [130,131], and raw lignocellulosic biomass [132,133]. The broad applicability of thiocracking is attributable to the homolytic ring-opening of sulfur and self-polymerization to form polymeric sulfur diradicals at >159 °C. These radical-terminated sulfur catenates react with both organic radicals and radical-reactive species that form when organics are heated, allowing diverse reactivity with a range of functional groups (Figure 1). Thiocracking is thus an attractive method for the potential single-stage, one-pot, atom-economic conversion of mixed-material waste streams.

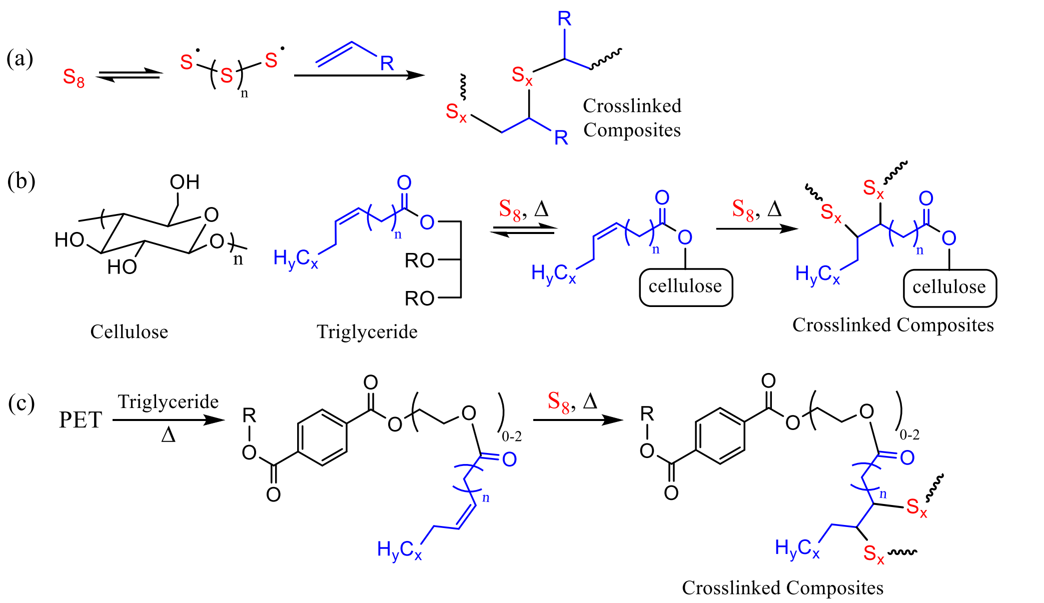

Figure 1. Heating organics with elemental sulfur facilitates formation of S–C bonds via vulcanization (**a**). This can occur in one-pot methods with concomitant transesterification between triglycerides and cellulose (**b**) or poly(ethylene terephthalate) (**c**). The resultant crosslinked composites can have over twice the compressive strength of ordinary Portland cement (OPC).

The objective of the current study is to demonstrate that thiocracking is a viable method for upcycling challenging multi-materials that (1) are difficult to physically separate into their individual components, (2) comprise challenging mixtures of plastic, paper, and food waste, and (3) are produced in high volume. Post-consumer peanut butter jars meet all of these criteria. Peanut butter is popular globally, with consumption worldwide projected to increase by 36% between 2023 and 2028, and over 612 million jars of peanut butter are already produced annually in the United States alone [134]. Other than removing the lid, it is difficult to physically separate any of the other components of a post-consumer peanut butter jar: the induction seal and label are attached with adhesive and residual peanut butter sticks tenaciously to the sides of the jar, making it a prototypically challenging multi-material for the current study (Figure 2).

Previous investigations into the preparation of composites via reaction of elemental sulfur with triglycerides, PET, polysaccharides, or combinations thereof (*vide infra*) suggested that a more complicated mixture of such chemical components may give similar high-strength composites. For these reasons, a peanut butter jar was selected as a food waste container having triglycerides (representative of fat in various food wastes) and cellulose (to represent polysaccharides present in many food wastes), and PET as a high-volume plastic waste.

Figure 2. Food packaging items are examples of multi-materials posing challenges for chemical recycling. A post-consumer peanut butter jar (**a**), for example, is made up of a polypropylene lid, a poly(ethylene terephthalate) (PET) jar body, a coated paper label, an induction seal (aluminum foil, wax, adhesive and pulpboard), and residual peanut butter (primarily triglycerides). Of the components (**b**), only the lid is easy to physically separate from the other components.

Herein, we report the thiocracking of a post-consumer peanut butter jar material with elemental sulfur to yield the composite $PBJS_{90}$, which has 2.2 times the compressive strength required for residential building foundations. Composite $PBJS_{90}$ is prepared entirely from waste materials with 100% atom economy, a remarkably low *E* factor [135] of 0.02, and a negative global warming potential of −0.099 kg CO_2e/kg.

2. Materials and Methods

2.1. Instrumentation and Calculations

Proton NMR spectra were acquired on a Bruker NEO-300 MHz (Bruker, Billerica, MA, USA) at room temperature and data processed with MestReNova x64-14.3-30573 software. All spectra reported were calibrated to the residual solvent peak from deuterated chloroform. Fourier transform infrared spectra were obtained using a Shimadzu IR Affinity-

1S (Shimadzu Corporation, Columbia, MD, USA) instrument with an ATR attachment operating over 400–4000 cm^{-1} at ambient temperature. UV-Vis data were collected on an Agilent Technologies Cary 60 UV-Vis (Agilent Technologies, Inc., Santa Clara, CA, USA) using Simple Reads software (Cary WinUV Scan Application Version 5.1.0.1016). SEM and EDX were acquired on a Schottky Field Emission Scanning Electron Microscope SU5000 (Hitachi High-Tech, Tokyo, Japan) operating in variable pressure mode with an accelerating voltage of 15 keV.

Thermogravimetric analysis (TGA) data were recorded on a TA SDT Q600 (TA Instruments, New Castle, DE, USA) instrument over the range 25 to 800 °C, with a heating rate of 10 °C·min^{-1} under a flow of N_2 (20 mL min^{-1}). DSC data were acquired (Mettler Toledo DSC 3 STARe System, Mettler Toledo, Columbus, OH, USA) over the range −60 to 140 °C with a heating rate of 10 °C·min^{-1} under a flow of N_2 (200 mL·min^{-1}). Each DSC measurement was carried out over three heat–cool cycles. For percentage crystallinity calculations, T_m, ΔH_m and ΔH_cc, the data were taken from the third heat/cool cycles. Melting enthalpies and cold crystallization enthalpies were calculated using DSC data. The reduction in the percentage crystallinity of the composite $PBJS_{90}$ with respect to sulfur was calculated using the following equation.

$$\Delta\chi_c = 1 - \left\{ \frac{\Delta H_{m(PBJS_{90})} - \Delta H_{cc(PBJS_{90})}}{\Delta H_{m(S)} - \Delta H_{cc(S)}} \right\} \times 100\%$$

where the variables are defined as follows:

$\Delta\chi_c$ Change in percentage crystallinity with respect to sulfur
$\Delta H_{m(PBJS_{90})}$ Melting enthalpy of composite materials ($PBJS_{90}$)
$\Delta H_{cc(PBJS_{90})}$ Cold crystallization enthalpy of composite materials
$\Delta H_{m(S)}$ Melting enthalpy of sulfur
$\Delta H_{cc(S)}$ Cold crystallization enthalpy of sulfur

Compressive strength analysis was performed on a Mark-10 ES30 (Mark-10 Corporation, Copiague, NY, USA) test stand equipped with a M3-200 force gauge (1 kN maximum force with ±1 N resolution) with an applied force rate of 3–4 N·s^{-1}. Compression cylinders were cast from silicone resin molds (Smooth-On Oomoo® 25 tin-cure, Oomoo Corp, Richmond, BC, Canada) with diameters of approximately 6 mm and heights of approximately 10 mm. Samples were manually sanded to ensure uniform dimensions and measured with a digital caliper with ±0.01 mm resolution. Compressional analysis was performed in triplicate, and the results were averaged. Flexural strength analysis was performed using a Mettler Toledo DMA 1 STARe System (Mettler Toledo, Columbus, OH, USA) in single cantilever mode. The samples were cast from silicone resin molds (Smooth-On Oomoo® 25 tin-curve, Oomoo Corp, Richmond, BC, Canada). The sample dimensions were approximately 1.5 mm × 15 mm × 23 mm. Flexural analysis was performed in triplicate and the results were averaged. The clamping force was 1 cN·m.

2.2. Preparation of Jar for Thiocracking

Whereas the jar (without the lid) eventually used for thiocracking was ground without separating the components, another identical jar was first analyzed to assess its components and their contribution to the jar. A post-consumer peanut butter jar was thus physically deconstructed and the peanut butter residue was recovered from the jar by rinsing with hexanes followed by removal of hexanes by rotary evaporation under reduced pressure. The mass of each component was recorded to allow calculation of each component's contribution to the overall mass (Table 1). Each individual component was analyzed by FTIR spectroscopy (Supplementary Materials Figures S4–S9), TGA (Supplementary Materials Figures S14–S17), and DSC (Supplementary Materials Figures S19–S22). An identical post-consumer jar of peanut butter was taken without the lid as the organic component for use in the thiocracking process. The difference in mass between the two identical jars was assumed to be the difference in peanut butter residue remaining in the jar. The jar for thiocracking was placed in a blender and processed for several minutes to produce a coarse aggregate. The mixture was then added in small batches to a coffee grinder to produce the fine aggregate (PBJ) used as the organic component in thiocracking.

Table 1. Mass breakdown of each component of PBJ and the primary constituents of each component.

Component	Mass	% of Upcycled Mass	Primary Chemical Components
Jar Without Lid	38.800 g	100%	Muti-Material (breakdown below)
Induction Seal	0.265 g	0.68%	Aluminum, cellulose, wax, polymer(s)
Adhesive	0.020 g	0.05%	Acrylic/rubber polymer(s)
Label	1.473 g	3.79%	Cellulose
Residual Peanut Butter	15.482 g	39.9%	Triglycerides
Jar Body	21.560 g	55.6%	Poly(ethylene terephthalate)

2.3. Synthesis

CAUTION: Heating elemental sulfur with organics can result in the formation of H_2S or other gases. Such gases can be toxic, foul-smelling, and corrosive. The temperature must be carefully controlled to prevent thermal spikes, contributing to the potential for H_2S or other gas evolution. Rapid stirring shortened heating times, and very slow addition of reagents can help avoid unforeseen temperature spikes.

2.3.1. Preparation of $PBJS_{90}$

To a Parr bomb reactor were added 13.5 g (0.053 mol) elemental sulfur and 1.50 g PBJ. The reactor was heated to 320 °C and allowed to run for 2 h before cooling to room temperature and the composite was removed from the reactor, giving the composite as a black matte solid in quantitative yield. Upon completion of this reaction, no mass was observed, indicating this reaction proceeded with 100% atom economy. Two batches of $PBJS_{90}$ were prepared and metrics were identical within statistical error.

2.3.2. Heating of PBJ in the Absence of Sulfur to Give hPBJ

In a glovebox under an atmosphere of dry $N_2(g)$ was added approximately 5 g of PBJ to the Parr bomb reactor. The reactor was heated to 320 °C for 2 h before cooling to room temperature to yield 3.10 g of hPBJ as a non-remeltable, heterogeneous solid comprising a mixture of light- and dark-colored particles.

2.3.3. Depolymerization of $PBJS_{90}$

In a glovebox under an atmosphere of dry $N_2(g)$ was added 100 mg $PBJS_{90}$ and 175 mg $LiAlH_4$ to a glass vial equipped with a magnetic stir bar. The solid mixture was suspended in 7 mL anhydrous toluene and sealed with a rubber septum. The reaction was stirred for 24 h at room temperature. At the conclusion of the reaction time, the reaction vessel was removed from the glovebox and placed in an ice bath under a flow of N_2 gas. The reaction was slowly quenched with 5% (*v*/*v*) HCl:ethanol until no more evolution of hydrogen gas was observed. The solution was washed with HCl(*aq*) (pH = 5) three times. The organic layer was separated, and the solvent removed by rotary evaporation under reduced pressure, yielding 23 mg of the yellow solid *d*-$PBJS_{90}$.

2.4. Determination of Dark Sulfur Content

To determine the dark sulfur content, a modified literature method for quantification by UV-vis spectroscopy in ethyl acetate was employed [136]. To a 250 mL volumetric flask was added 6.7 mg $PBJS_{90}$ (weighed with a microbalance) and approximately 230 mL ethyl acetate. The mixture was allowed to stir for 30 min after which the solution was made up to the mark of 250 mL with ethyl acetate. A 3 mL aliquot of this solution was transferred to a cuvette and 3 mL pure ethyl acetate was transferred to a separate cuvette to serve as a blank. Data were collected at 275 nm and the dark sulfur content calculated from a calibration curve having the equation $y = 36.124x + 0.012$ ($R^2 = 0.9967$), where y is the absorbance and x is the concentration of sulfur in mg/mL.

2.5. Mechanical Strength Analysis

Cylinders with diameters of approximately 6 mm and heights of approximately 10 mm, appropriate for compressive strength measurements, were prepared by melting the composite at 160 °C, then slowly and carefully poured into molds and allowed to solidify. Samples were stored at room temperature for 4 d prior to strength measurements. The samples were sanded to remove flack and measured with a digital caliper with a ±0.01 mm resolution.

3. Results and Discussion

3.1. Design and Preliminary Analysis of Multi-Material

In this study, the overarching goal was to assess the extent to which a simple, single-stage thiocracking process could be applied to a representative post-consumer mixed waste packaging item comprising waste plastic, paper, adhesives/seals and food waste. As a test item for this proof-of-principle study, a post-consumer jar (total weight = 47.247 g) that when purchased by the consumer was filled with peanut butter was selected. The jar contained residual peanut butter waste that had been left by the consumer. All components were adhered to the main jar body other than the lid, which was physically removed and was not used for the subsequent steps of the study. Although an entire jar (without the lid) was used for the thiocracking procedure, another identical jar was separated so that its individual components could be analyzed and the percentage composition by mass of each component quantified (Table 1).

The jar had contained 510 g of peanut butter when purchased, and the post-consumer jar contained 15.482 g of residual peanut butter (3.0% of purchased product). The residual peanut butter, primarily composed of triglycerides, and the jar body, composed of poly(ethylene terephthalate) (PET), were determined to be the two majority components (>95 wt. % of thiocracked organics) of the jar. The minority components (<5 wt. % of thiocracked organic mass) were the label (primarily cellulose), the induction seal (aluminum foil, wax, polymer coating, and pulp board), and the adhesive (acrylic and rubber polymers), collectively accounting for <5% of the thiocracked mass. Preliminary analysis of each component of the jar was carried out using infrared spectroscopy, thermogravimetric analysis, differential scanning calorimetry, and, for soluble components, proton nuclear magnetic resonance (^{1}H NMR) spectrometry. These analyses further validate the identity of each component and provide points of comparison for the derivative composite discussed below. The data for each component from each of these techniques are provided in the Supplementary Materials File as Figures S1, S4–S9, S14–S17 and S19–S22.

Olefins found in the peanut butter residue triglycerides are expected to undergo inverse vulcanization (addition of sulfur across C–C π bonds, as shown in Figure 1a) during thiocracking [93,137–141]. The total olefin content contributed by the residue was thus quantified by ^{1}H NMR spectrometry with 2,3,4,5,6-pentafluorobenzaldehyde added as an internal standard (Figure S2). Calculations based on the ratio of integration of the alkene region (4.5–5.5 ppm) versus the aldehydic proton resonance on the internal standard (10.3 ppm) indicated an olefin content of 4.3 mmol·g^{-1} for the peanut butter residue alone and an olefin content of 1.7 mmol·g^{-1} for the jar used in thiocracking.

3.2. Reactivity of Individual Components with Elemental Sulfur

We have undertaken several studies to understand the reactivity of the primary individual jar components with elemental sulfur under thiocracking conditions. Triglycerides, the primary constituent of the peanut butter residue, undergo inverse vulcanization to give composites as previously reported (Figure 1a) [142]. At the temperatures used for thiocracking, triglycerides also undergo transesterification reactions with both PET [125] and cellulose (the primary constituent of paper) [132,133]. In the case of PET, this transesterification was demonstrated to lead to its depolymerization into oligomers of fatty acid-functionalized terephthalate derivatives [125]. Cellulose derivatized with olefins, as by transesterification with triglycerides in the current case, also reacts with sulfur to give composites formed via crosslinking of olefins by sulfur [130,143]. Analogous tandem depolymerization/transesterification/vulcanization of the mixed-material jar components in the current case is likewise responsible for forming homogeneous composites comprising structures shown in Figure 1b,c.

3.3. Thiocracking and Chemical Analysis of Composite $PBJS_{90}$

The post-consumer peanut butter jar without the polypropylene lid was converted into a mixture by coarse grinding in an industrial blender followed by comminution in a coffee grinder to give the finely ground pulp (PBJ, Figure 3a) used in the thiocracking process. Composite $PBJS_{90}$ was then prepared by heating PBJ (10 wt. %) with elemental sulfur (90 wt. %) at 320 °C in a stainless-steel autoclave for 2 h (Figure 3b). This process yielded a black, glassy material of low viscosity which remained shiny once cooled, that was readily shaped by pouring the molten material into a silicone mold and allowing it to cool to room temperature (Figure 3b). In contrast, when ground PBJ is heated under the same conditions, the product is a brittle, heterogeneous solid comprising a mixture of light- and dark-colored particles. This solid is not remeltable and cannot readily be shaped.

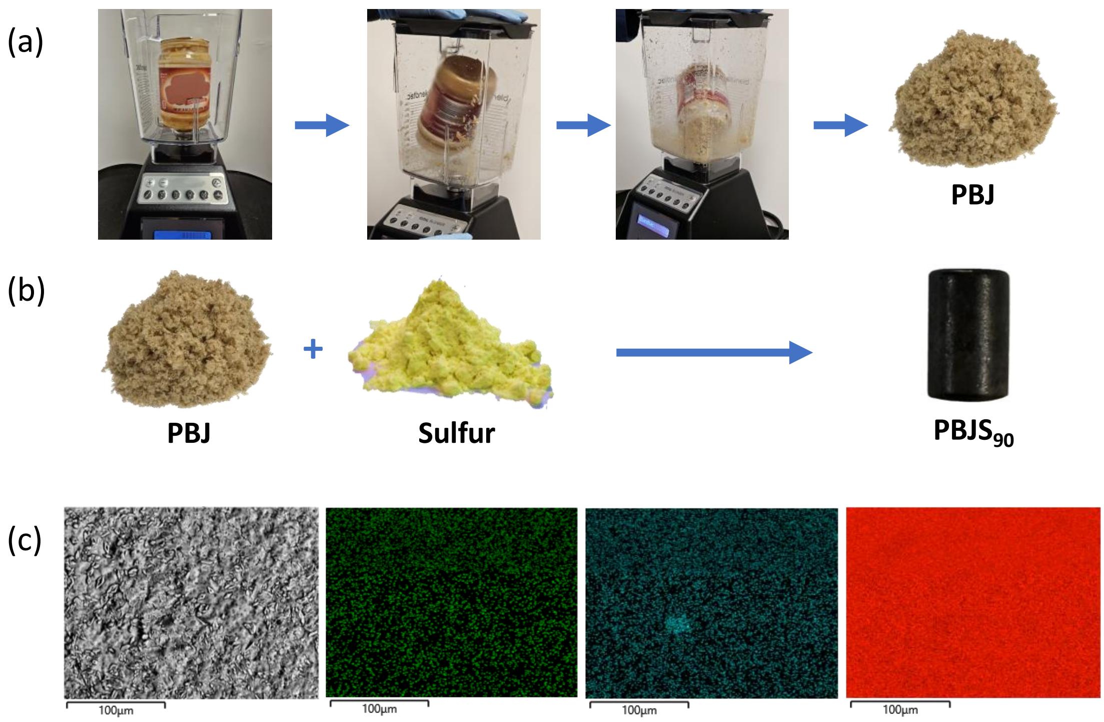

Figure 3. Breakdown of post-consumer jar (**a**) for use in thiocracking to give black composite $PBJS_{90}$ (**b**). Imaging (**c**) of $PBJS_{90}$ by scanning electron microscopy (SEM, gray image) with elemental mapping by energy dispersive X-ray analysis (EDX) where carbon is shown in green, oxygen in blue, and sulfur in red.

High sulfur-content materials (HSMs) can be depolymerized by their reaction with $LiAlH_4$, which leads to breakage of S–S bonds and consequent conversion of the S–C crosslink points to thiols. $PBJS_{90}$ was depolymerized in this way to give *d*-$PBJS_{90}$. Because only a single thiol sulfur remains in *d*-$PBJS_{90}$ where each polysulfur crosslinking chain ($–S_x–$ in Figure 1) had been in $PBJS_{90}$, the majority of the 90 wt. % sulfur is removed, thus improving the spectroscopic signal-to-noise ratio for characterization of organics in the material, as was readily demonstrated by IR spectra for $PBJS_{90}$ and *d*-$PBJS_{90}$ (Figures S3, S11 and S13 in Supplementary Materials). Infrared spectra for $PBJS_{90}$ and *d*-PBJS_{90} showed evidence of the anticipated S–C bond formation by a broad S–C stretch at 728 cm^{-1} in PBJS_{90} and *d*-PBJS_{90}. Further evidence of microscale homogeneity was obtained by imaging a film of PBJS_{90} by scanning electron microscopy with elemental mapping by energy dispersive X-ray (SEM/EDX). These images showed an even distribution of carbon, oxygen, and sulfur throughout the material, and no evidence of gross phase separation throughout the surface of the material on a 100 μm scale (Figure 3c).

Although no distinct small molecules were identified from the complex mixture resulting from the thiocracking of the mixed waste in the current study, several prior studies were undertaken to understand the chemistry of the components under these reaction conditions. For example, we have previously reported detailed studies on the reactions of elemental sulfur with (1) triglycerides [142,144], (2) polysaccharides (cellulose and starch) [129,131], (3) lignocellulosic biomass [132,133], (4) mixtures of peanut oil with polysaccharides (starch or cellulose) [145], and (5) PET with triglycerides [123,125]. These studies revealed that (1) triglycerides undergo transesterification with polysaccharides and PET, (2) sulfur adds across the pi bonds in triglyceride-derived olefins. All three classes of components—triglycerides, polysaccharides, and PET—are present in the organic monomer feed for PBJS90, leading to the formulation of the chemical structure as shown in Figure 4.

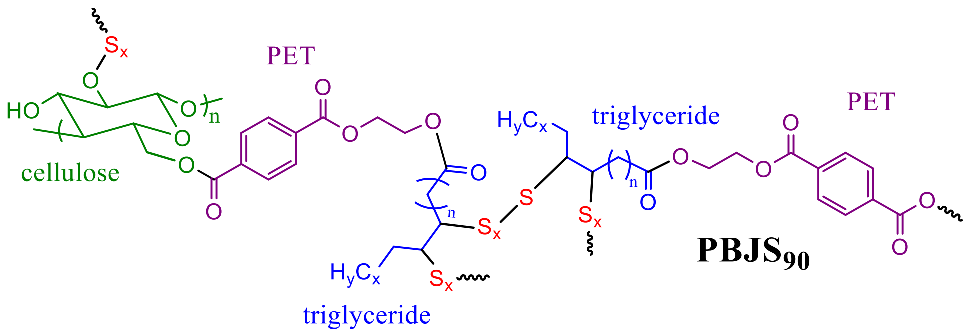

Figure 4. Representative structural features of PBJS_{90} derived from the primary jar components of cellulose, triglycerides, and PET.

The sulfur in composites like PBJS_{90} is usually present as crosslinking polysulfur catenates (–S_x– in Figure 1) that are covalently attached to the organic molecules and some physically entrapped oligosulfur species known as "dark sulfur" [146]. The presence of larger quantities of dark sulfur generally leads to poorer mechanical strength in high sulfur content composites. To further validate the chemical composition of PBJS_{90}, the amount of dark sulfur in PBJS_{90} was quantified by UV-Vis spectroscopy by the published method [136]. This analysis revealed a dark sulfur content of only 14 wt. % in PBJS_{90}. Despite the high PET content in PBJS_{90}, its dark sulfur content is more similar to sulfur composites made from triglyceride mixtures (e.g., CanBG_{90} made from 90 wt. % sulfur, 5 wt. % brown grease and 5 wt. % canola oil, and having 14% dark sulfur content) [144] than to composites made from PET and sulfur, for example the 82% dark sulfur content in SPG (90 wt. % sulfur with 10 wt. % geraniol/PET derivative) [49] or 88% dark sulfur content in mPES (90 wt. % sulfur with 10 wt. % oleyl-derivatized PET) [123]. The low dark sulfur content in PBJS_{90} predictably trends with its high compressive strength, as discussed in the following section.

3.4. Thermal and Mechanical Properties

Thermogravimetric analysis (TGA and DTGA, Table 2 and Figures S14–S18 in the Supplementary Materials) showed a single T_d (here defined as the temperature at which 5% mass loss is observed) at 218 °C in PBJS_{90}. This value is slightly lower than the T_d observed for *cyclo*-S_8 (229 °C) and is attributable to sublimation of sulfur—from both dark sulfur and decomposing polysulfur crosslinking chains—out of the material. TGA thermograms for PBJ components (Figures S14–S18 in the Supplementary Materials) revealed higher T_d values than that observed in PBJS_{90}. No additional thermal features attributable to unreacted individual jar components (PET, cellulose, etc.) were observable, providing further evidence of the established transesterification/vulcanization pathways expected for the triglyceride, cellulose, and PET components comprising >99% of the organic content of $PBJS_{90}$ (Figure 1).

Table 2. Thermal and morphological properties of mixed composition waste and sulfur composite $PBJS_{90}$ with comparison to elemental sulfur.

Material	T_d [a] °C	T_m [b] °C	T_g [c] °C	Cold Crystal. Peaks/°C	ΔH_m J/g	ΔH_{cc} J/g	Percent Crystallinity [d]	Dark Sulfur (%) [e]
$PBJS_{90}$	218	117	NA	36	27	–5	29	14
S_8	229	118	NA	NA	44.8	NA	100	0

[a] The temperature at which the 5% mass loss was observed. [b] The temperature at the peak maximum of the endothermic melting from the third heating cycle. [c] Glass transition temperature. [d] The reduction in percentage crystallinity of each sample was calculated with respect to sulfur (normalized to 100%). [e] Percentage of extractable sulfur calculated from UV-vis data according to a modified literature procedure [136].

Thermomorphological changes in the composite $PBJS_{90}$ were also evaluated by differential scanning calorimetry (DSC, Table 2 and Figures S19–S23). DSC thermograms also showed a cold crystallization peak at 36 °C and a melting feature at 117 °C for $PBJS_{90}$. The percentage crystallinity calculated from melting and cold crystallization enthalpies of $PBJS_{90}$ was determined to be 29%, indicating there are some crystalline regions present but that the material is primarily composed of amorphous materials, consistent with the presence of amorphous $–S_x–$ crosslinking chains.

Cylinders for compressive strength analysis were prepared by melting $PBJS_{90}$ at 180 °C and pouring the material into molds. Samples were allowed to sit for 96 h prior to testing, following the convention for high sulfur-content materials with 90 wt. % sulfur content for compressive strength analysis [129]. The compressive strength of $PBJS_{90}$ was found to be 37.7 ± 2.9 MPa (Table 3, Figure S25, stress strain plots in Figure S24 of the Supplementary Materials), over 200% stronger than that required of OPC for use in residential building foundations. $PBJS_{90}$ exhibits exceptional compressive strengths, exceeding that of other high sulfur-content materials comprised of similar materials such as APS_{95} (35.7 MPa), SPG (23.1 MPa), and mPES (26.9 MPa). $PBJS_{90}$ also exceeds the mechanical properties of other cement materials containing plastics or plastic aggregates (Table 3).

Table 3. Mechanical properties of $PBJS_{90}$ compared to other high sulfur-content materials, materials containing recycled plastics, and commercially available building materials.

Sample	Compressive Strength (MPa)	After Acid (MPa)	Strength Retained (%)	Compressive Modulus	Flexural Strength (MPa)	Flexural Modulus
$PBJS_{90}$	37.7 ± 2.9	35.4 ± 4.5	94%	74 ± 5	5.64 ± 0.32	631 ± 20.8
APS_{95} [a]	35.7	ND [h]	ND	ND	4.8	690
SPG [b]	23.1	ND	ND	ND	4.7	ND
mPES [c]	26.9	ND	ND	ND	7.7	ND
Brick 1 [d]	11.2	ND	ND	ND	ND	ND
Brick 2 [e]	16.4	ND	ND	ND	2.75	ND
Brick 3 [f]	9.0	ND	ND	ND	ND	ND
C62 Brick [g]	8.6	ND	ND	ND	ND	ND
OPC	17	ND	ND	ND	3.7	580

[a] Composite of allylated peanut shells (5 wt. %) and sulfur (95 wt. %) [132] [b] Composite of PET (5 wt. %), geraniol (5 wt. %), sulfur (90 wt. %) [49] [c] Composite of glycolyzed PET (10 wt. %) and sulfur (90 wt. %) [123] [d] Brick with HDPE from physical recycling via melting and compression [147] [e] Brick with 85% fine PVC aggregate in cement [148] [f] Brick of OPC with 10% mixed plastic waste aggregate, cement optimized [149] [g] Brick classification C62 for building brick with negligible weathering. [h] ND = not determined in the reported paper.

Whereas mineral-based legacy building materials show significant degradation upon exposure to acidic conditions, previous studies on high sulfur-content materials demonstrate that they often show impressive resistance to corrosion by acids. To investigate the corrosion resistance of $PBJS_{90}$, its compressive strength was remeasured following submersion in 0.5 M H_2SO_4 for 24 h. After this acid challenge, the compressive strength was determined to be 35.4 $\pm$ 4.5 MPa, indicating that $PBJS_{90}$ retained 94% of its strength under conditions that will completely dissolve OPC. $PBJS_{90}$ also displays an exceptionally low 0.14% uptake of water following 24 h of submersion (cf. 28% for OPC) [129]. Low water uptake is another important metric for weathering resistance, as seasonal freezing and thawing cause expansion–contraction cycling of absorbed water that leads to a crack formation and is a primary mechanism for OPC failure in temperate climates [150].

The flexural strength of $PBJS_{90}$ was determined through dynamic mechanical analysis in a single cantilever mode. Rectangular prisms were prepared by pouring material into a mold and subsequent manual sanding to a thickness of 1.4 mm. $PBJS_{90}$ was found to have a flexural strength of 5.64 $\pm$ 0.32 MPa, and a flexural modulus of 631 $\pm$ 20.8. This falls within the range of other high sulfur-content materials (Table 3), and exceeds that of average flexural strength values observed by OPC.

3.5. Environmental and Sustainability Impact Analysis

If the goal is to replace OPC with $PBJS_{90}$, some assessment of the environmental impact of the two materials will be insightful. The *E* factor [135] is a common metric for estimating the relative environmental impact of a material in which the focus is on the amount of waste produced versus the amount of useful product obtained. The *E* factor is equal to the mass of waste produced divided by the mass of useful product produced, such that a lower *E* factor indicates lower relative waste generation. The *E* factors for commercial bulk chemicals range from <1 to over 50 [151,152]. If we consider the inputs to making $PBJS_{90}$ to be sulfur and the jar with its lid, we calculate the *E* factor (using masses for one whole jar with the lid as delineated in Table 1) as:

$$E\ factor = \frac{waste}{useful\ product} = \frac{lid}{(lidless\ jar + sulfur)} = \frac{8.45\ \text{g}}{(38.8\ \text{g} + 349\ \text{g})} = 0.02$$

The *E* factor for $PBJS_{90}$ is nearly two orders of magnitude lower than that of OPC (1.4) [151]. The conversion of the lidless jar and sulfur to $PBJS_{90}$ proceeds with 100% atom economy (no lost mass within error), so the only waste of the process is the lid. Since the lid was already discarded as waste by the consumer of the peanut butter, the net waste to the environment is approximately zero.

A potential shortcoming of the *E* factor and atom economy metrics is that they focus on the mass/atom balance and do not account for energy consumption or net carbon dioxide emission. For this purpose, it is instructive to determine the global warming potential, an estimate of kilograms of CO_2 emitted per kilogram of useful material made (kg CO_2e/kg). In the current case, a low global warming potential of -0.099 kg CO_2e/kg was calculated for $PBJS_{90}$, making its preparation slightly carbon-offsetting (estimates, assumptions, and inputs for these calculations are provided in the Supplementary Materials). This compares to a much higher value of 1.0 kg CO_2e/kg for OPC. Not only is the global warming potential of OPC quite high, but OPC is also the most-produced synthetic good by mass, such that its manufacture is responsible for ~8% of all anthropogenic CO_2 production, similar to or exceeding the amount produced by noncommercial automobile transportation [153–157]. These data emphasize the need for waste-derived cements or geopolymer cements [158–160] to replace OPC as elements of the built environment as a significant measure against runaway CO_2 production in the future.

The work described herein contributes positively to achieving several United Nations Sustainable Development Goals (SDGs). The work described herein advances SDG 12: Responsible Consumption and Production by demonstrating a single-stage method for converting complex, multi-material post-consumer packaging into high-strength composites, thereby potentially reducing waste and promoting more sustainable material lifecycles. The resultant composites have a negative global warming potential so if these composites could be used as alternatives to traditional building materials, this would contribute to reduced carbon emissions, directly supporting SDG 13: Climate Action. The utilization of waste-derived inputs underscores the relevance to SDG 9: Industry, Innovation, and Infrastructure. Furthermore, the ecological benefits, including the reduction in microplastic pollution, align with SDG 14: Life Below Water and SDG 15: Life on Land. New technologies come with their own challenges, and the environmental impact of the composites will need to be thoroughly explored before their widespread use, but this proof-of-concept study holds promise for a more sustainable future.

4. Conclusions

With the quantity of single-use packaging components being deposited into landfills rising exponentially faster than recycling, it is crucial to develop versatile methods to address the challenges currently present in recycling mixed-composition waste. The proof-of-principle study reported herein demonstrates the first utility of thiocracking for recycling consumer waste products of mixed composition through its reaction with fossil fuel refining byproduct sulfur. The resulting composite, $PBJS_{90}$, was prepared with a low *E* factor, 100% atom economy, and a negative global warming potential of -0.099 kg CO_2e/kg. The composite showed a compressive strength greater than 200% of that required for building foundations and flexural strengths also exceeding that of ordinary Portland cement, a material with a high global warming potential of 1.0 kg CO_2e/kg. The process and materials described herein may support UN SDGs 9 and 12–15 in humanity's quest for a more sustainable future. The attractive properties of $PBJS_{90}$ suggest its potential as a greener alternative to legacy mineral-based structural materials, pending, of course, results of long-term environmental impact and weathering studies. Nonetheless, this proof-of-principle study holds promise for the use of thiocracking to effectively recycle mixed waste comprised of various plastics, food remnants, greases, cellulose-based materials, and other contaminants to durable structural goods.

Supplementary Materials: The following supporting information can be downloaded at: https://www.mdpi.com/article/10.3390/su16167023/s1, Figure S1. Proton NMR spectrum (300 MHz, $CDCl_3$) of adhesive holding the label to the jar. Figure S2. Proton NMR spectrum (300 MHz, $CDCl_3$) of peanut butter residue with 2,3,4,5,6–pentafluorobenzaldehyde (exhibiting a single resonance at 10.29 ppm) added as internal standard. Figure S3. FT–IR spectra for $PBJS_{90}$ (black trace) and *d*–$PBJS_{90}$ (gray trace) emphasizing the S–C stretch at 728 cm^{-1}. The Full IR spectrum for these as well each individual jar component are provided in Figures S4–S13. Figure S4. Full IR spectrum of peanut butter jar over a range of 4000 to 600 cm^{-1}. The feature observed between 1900 and 2400 cm^{-1} is an artifact of the ATR attachment. Figure S5. Full IR spectrum of lid removed from the peanut butter jar over a range of 4000 to 600 cm^{-1}. The feature observed between 1900 and 2400 cm^{-1} is an artifact of the ATR attachment. Figure S6. Full IR spectrum of the inside of the label removed from peanut butter jar over a range of 4000 to 600 cm^{-1}. The feature observed between 1900 and 2400 cm^{-1} is an artifact of the ATR attachment. Figure S7. Full IR spectrum of the outside of the label removed from peanut butter jar over a range of 4000 to 600 cm^{-1}. The feature observed between 1900 and 2400 cm^{-1} is an artifact of the ATR attachment. Figure S8. Full IR spectrum of paper side of the induction seal removed from peanut butter jar over a range of 4000 to 600 cm^{-1}. The feature observed between 1900 and 2400 cm^{-1} is an artifact of the ATR attachment. Figure S9. Full IR spectrum of the foil side of the induction seal removed from peanut butter jar over a range of 4000 to 600 cm^{-1}. The feature observed between 1900 and 2400 cm^{-1} is an artifact of the ATR attachment. Figure S10. Full IR spectrum of $PBJS_{90}$ over a range of 4000 to 600 cm^{-1}. The feature observed between 1900 and 2400 cm^{-1} is an artifact of the ATR attachment. Figure S11. Full IR spectrum of the insoluble fraction of $PBJS_{90}$ over a range of 4000 to 600 cm^{-1}. The feature observed between 1900 and 2400 cm^{-1} is an artifact of the ATR attachment. Figure S12. Full IR spectrum of hPBJ over a range of 4000 to 600 cm^{-1}. The feature observed between 1900 and 2400 cm^{-1} is an artifact of the ATR attachment. Figure S13. Full IR spectrum of *d*–$PBJS_{90}$ over a range of 4000 to 600 cm^{-1}. The feature observed between 1900 and 2400 cm^{-1} is an artifact of the ATR attachment. Figure S14. Mass loss curve and DTGA from thermogravimetric analysis for the PET jar body over the range 25–800 °C. Figure S15. Mass loss curve and DTGA from thermogravimetric analysis for the lid over the range 25–800 °C. Figure S16. Mass loss curve and DTGA from thermogravimetric analysis for the label over the range 25–800 °C. Figure S17. Mass loss curve and DTGA from thermogravimetric analysis for the induction seal over the range 25–800 °C. Figure S18. Mass loss curve and DTGA from thermogravimetric analysis for $PBJS_{90}$ over the range 25–800 °C. Figure S19. Thermogram from differential scanning calorimetry (endothermic down) for the PET jar body over the range −60–140 °C. Figure S20. Thermogram from differential scanning calorimetry (endothermic down) for the lid over the range −60–140 °C. Figure S21. Thermogram from differential scanning calorimetry (endothermic down) for the label over the range −60–140 °C. Figure S22. Thermogram from differential scanning calorimetry (endothermic down) for the induction seal over the range −60–140 °C. Figure S23. Thermogram from differential scanning calorimetry (endothermic down) for $PBJS_{90}$ over the range −60–140 °C. Figure S24. Stress–strain plots for measurements of the compressive strength of $PBJS_{90}$ as prepared (top, 37.7 ± 2.9 MPa) and after acid challenge (bottom, 35.4 ± 4.5MPa). Figure S25. Compressive strength for $PBJS_{90}$ before and after acid exposure compared to bricks incorporating recycled plastic (Bricks 1–3), commercial building brick of classification C62, OPC, and other high sulfur content materials. Materials APS_{95}, SPG, mPES, and Bricks 1–3 are as defined in the footnote in Table 3. Figure S26. Stress–strain curve of $PBJS_{90}$ determined during flexural strength testing. The orange dotted line represents the propagations of the linear regions of the stress–strain curve used to determine the flexural modulus. References [161–170] are citied in the Supplementary Materials.

Author Contributions: The authors primarily responsible for particular CRediT roles are provided here. K.M.D.: Data curation, Formal analysis, Investigation, Validation, Roles/Writing—original draft. R.C.S.: Conceptualization, Methodology, Resources, Supervision, Roles/Writing—review and editing. All authors have read and agreed to the published version of the manuscript.

Funding: This research was funded by The National Science Foundation grant number CHE-2203669 to R.C.S.

Informed Consent Statement: Not applicable.

Data Availability Statement: The original contributions presented in the study are included in the article/Supplementary Materials; further enquiries can be directed to the corresponding author.

Conflicts of Interest: The authors declare no conflicts of interest.

References

1. Thiounn, T.; Smith, R.C. Advances and approaches for chemical recycling of plastic waste. *J. Poly. Sci.* **2020**, *58*, 1347–1364. [CrossRef]
2. Krausmann, F.; Schaffartzik, A.; Mayer, A.; Gingrich, S.; Eisenmenger, N. Global trends and patterns in material use. *MRS Online Proc. Libr.* **2013**, *1545*, mrss13-1545. [CrossRef]
3. Geyer, R.; Jambeck, J.R.; Law, K.L. Production, use, and fate of all plastics ever made. *Sci. Adv.* **2017**, *3*, e1700782. [CrossRef]
4. Fagnani, D.E.; Tami, J.L.; Copley, G.; Clemons, M.N.; Getzler, Y.D.Y.L.; McNeil, A.J. 100th Anniversary of Macromolecular Science Viewpoint: Redefining Sustainable Polymers. *ACS Macro Lett.* **2021**, *10*, 41–53. [CrossRef] [PubMed]
5. Pires, A.; Martinho, G. Waste hierarchy index for circular economy in waste management. *Waste Manag.* **2019**, *95*, 298–305. [CrossRef]
6. Oberoi, I.S.; Rajkumar, P.; Das, S. Disposal and recycling of plastics. *Mater. Today Proc.* **2021**, *46*, 7875–7880. [CrossRef]
7. Benyathiar, P.; Kumar, P.; Carpenter, G.; Brace, J.; Mishra, D.K. Polyethylene Terephthalate (PET) Bottle-to-Bottle Recycling for the Beverage Industry: A Review. *Polymers* **2022**, *14*, 2366. [CrossRef]
8. Bohre, A.; Jadhao, P.R.; Tripathi, K.; Pant, K.K.; Likozar, B.; Saha, B. Chemical Recycling Processes of Waste Polyethylene Terephthalate Using Solid Catalysts. *ChemSusChem* **2023**, *14*, e202300142. [CrossRef]
9. Clark, J.H.; Matharu, A.S. Waste to wealth using green chemistry. *Issues Environ. Sci. Technol.* **2013**, *37*, 66–82.
10. Jeong, J.; Choi, J. Adverse outcome pathways potentially related to hazard identification of microplastics based on toxicity mechanisms. *Chemosphere* **2019**, *231*, 249–255. [CrossRef]
11. Cole, M.; Lindeque, P.; Halsband, C.; Galloway, T.S. Microplastics as contaminants in the marine environment: A review. *Mar. Pollut. Bull.* **2011**, *62*, 2588–2597. [CrossRef] [PubMed]
12. Brandts, I.; Barria, C.; Martins, M.A.; Franco-Martinez, L.; Barreto, A.; Tvarijonaviciute, A.; Tort, L.; Oliveira, M.; Teles, M. Waterborne exposure of gilthead seabream (*Sparus aurata*) to polymethylmethacrylate nanoplastics causes effects at cellular and molecular levels. *J. Hazard. Mater.* **2021**, *403*, 123590. [CrossRef] [PubMed]

13. Hidalgo-Ruz, V.; Gutow, L.; Thompson, R.C.; Thiel, M. Microplastics in marine environment review of methods for identification and quantification. *Environ. Sci. Technol.* **2012**, *46*, 3060–3075. [CrossRef]
14. Jehanno, C.; Alty, J.W.; Roosen, M.; De Meester, S.; Dove, A.P.; Chen, E.Y.X.; Leibfarth, F.A.; Sardon, H. Critical advances and future opportunities in upcycling commodity polymers. *Nature* **2022**, *603*, 803–814. [CrossRef] [PubMed]
15. Lahtela, V.; Hyvarinen, M.; Karki, T. Composition of plastic fractions in waste streams: Toward more efficient recycling and utilization. *Polymers* **2019**, *11*, 69. [CrossRef] [PubMed]
16. Ogura, A. Microalgae and microplastic removal. *Purasuchikkusu* **2022**, *73*, 41–45.
17. Schwarzbauer, J.; Heim, S.; Brinker, S.; Littke, R. Occurrence and alteration of organic contaminants in seepage and leakage water from a waste deposit landfill. *Water Res.* **2002**, *36*, 2275–2287. [CrossRef] [PubMed]
18. Shah, A.A.; Hasan, F.; Hameed, A.; Ahmed, S. Biological degradation of plastics: A comprehensive review. *Biotechnol. Adv.* **2008**, *26*, 246–265. [CrossRef] [PubMed]
19. Venancio, C.; Melnic, I.; Tamayo-Belda, M.; Oliveira, M.; Martins, M.A.; Lopes, I. Polymethylmethacrylate nanoplastics can cause developmental malformations in early life stages of *Xenopus laevis*. *Sci. Total Environ.* **2022**, *806*, 150491. [CrossRef]
20. Zhao, T.; Tan, L.; Han, X.; Wang, X.; Zhang, Y.; Ma, X.; Lin, K.; Wang, R.; Ni, Z.; Wang, J.; et al. Microplastic-induced apoptosis and metabolism responses in marine Dinoflagellate, *Karenia mikimotoi*. *Sci. Total Environ.* **2022**, *804*, 150252. [CrossRef]
21. Zhou, X.-X.; He, S.; Gao, Y.; Chi, H.-Y.; Wang, D.-J.; Li, Z.-C.; Yan, B. Quantitative Analysis of Polystyrene and Poly(methyl methacrylate) Nanoplastics in Tissues of Aquatic Animals. *Environ. Sci. Technol.* **2021**, *55*, 3032–3040. [CrossRef]
22. Thomas, D.; Schuetze, B.; Heinze, W.M.; Steinmetz, Z. Sample preparation techniques for the analysis of microplastics in soil-a review. *Sustainability* **2020**, *12*, 9074. [CrossRef]
23. Boumanchar, I.; Chhiti, Y.; M'Hamdi Alaoui, F.E.; El Ouinani, A.; Sahibed-Dine, A.; Bentiss, F.; Jama, C.; Bensitel, M. Effect of materials mixture on the higher heating value: Case of biomass, biochar and municipal solid waste. *Waste Manag.* **2017**, *61*, 78–86. [CrossRef]
24. Bora, R.R.; Wang, R.; You, F. Waste Polypropylene Plastic Recycling toward Climate Change Mitigation and Circular Economy: Energy, Environmental, and Technoeconomic Perspectives. *ACS Sust. Chem. Eng.* **2020**, *8*, 16350–16363. [CrossRef]
25. Cepeliogullar, O.; Putun, A.E. A pyrolysis study for the thermal and kinetic characteristics of an agricultural waste with two different plastic wastes. *Waste Manag. Res.* **2014**, *32*, 971–979. [CrossRef]
26. Ephraim, A.; Minh, D.P.; Lebonnois, D.; Peregrina, C.; Sharrock, P.; Nzihou, A. Co-pyrolysis of wood and plastics: Influence of plastic type and content on product yield, gas composition and quality. *Fuel* **2018**, *231*, 110–117. [CrossRef]
27. Esmizadeh, E.; Khalili, S.; Vahidifar, A.; Naderi, G.; Dubois, C. Waste Polymethyl Methacrylate (PMMA): Recycling and High-Yield Monomer Recovery. In *Handbook of Ecomaterials*; Martínez, L.M.T., Kharissova, O.V., Kharisov, B.I., Eds.; Springer International Publishing: Cham, Switzerland, 2018; pp. 1–33.
28. Godiya, C.B.; Gabrielli, S.; Materazzi, S.; Pianesi, M.S.; Stefanini, N.; Marcantoni, E. Depolymerization of waste poly(methyl methacrylate) scraps and purification of depolymerized products. *J. Environ. Manag.* **2019**, *231*, 1012–1020. [CrossRef] [PubMed]
29. Idumah, C.I. Recent advancements in thermolysis of plastic solid wastes to liquid fuel. *J. Therm. Anal. Calorim.* **2022**, *147*, 3495–3508. [CrossRef]
30. Khatwa, M.A.; Salem, H.G.; Haggar, S.M. Building material from waste. *Can. Metall. Q.* **2005**, *44*, 339–350. [CrossRef]
31. Liu, Y.; Lu, X.-B. Chemical recycling to monomers: Industrial Bisphenol-A-Polycarbonates to novel aliphatic polycarbonate materials. *J. Polym. Sci.* **2022**, *60*, 3256–3268. [CrossRef]
32. Luo, X.; Zhan, J.; Mei, Q.; Zhang, S. Selective oxidative upgrade of waste polystyrene plastics by nitric acid to produce benzoic acid. *Green Chem.* **2023**, *25*, 6717–6727. [CrossRef]
33. Munyaneza, N.E.; Posada, C.; Xu, Z.; De Altin Popiolek, V.; Paddock, G.; McKee, C.; Liu, G. A Generic Platform for Upcycling Polystyrene to Aryl Ketones and Organosulfur Compounds. *Angew. Chem. Int. Ed.* **2023**, *62*, e202307042. [CrossRef] [PubMed]
34. Ozsin, G.; Putun, A.E. A comparative study on co-pyrolysis of lignocellulosic biomass with polyethylene terephthalate, polystyrene, and polyvinyl chloride: Synergistic effects and product characteristics. *J. Clean. Prod.* **2018**, *205*, 1127–1138. [CrossRef]
35. Salvilla, J.N.V.; Ofrasio, B.I.G.; Rollon, A.P.; Manegdeg, F.G.; Abarca, R.R.M.; de Luna, M.D.G. Synergistic co-pyrolysis of polyolefin plastics with wood and agricultural wastes for biofuel production. *Appl. Energy* **2020**, *279*, 115668. [CrossRef]
36. Tang, Y.; Huang, Q.; Sun, K.; Chi, Y.; Yan, J. Co-pyrolysis characteristics and kinetic analysis of organic food waste and plastic. *Bioresour. Technol.* **2018**, *249*, 16–23. [CrossRef] [PubMed]
37. Worch, J.C.; Dove, A.P. 100th Anniversary of Macromolecular Science Viewpoint: Toward Catalytic Chemical Recycling of Waste (and Future) Plastics. *ACS Macro Lett.* **2020**, *9*, 1494–1506. [CrossRef] [PubMed]
38. Zhang, X.; Lei, H.; Zhu, L.; Zhu, X.; Qian, M.; Yadavalli, G.; Wu, J.; Chen, S. Thermal behavior and kinetic study for catalytic co-pyrolysis of biomass with plastics. *Bioresour. Technol.* **2016**, *220*, 233–238. [CrossRef] [PubMed]
39. Kugelmass, L.H.; Tagnon, C.; Stache, E.E. Photothermal Mediated Chemical Recycling to Monomers via Carbon Quantum Dots. *J. Am. Chem. Soc.* **2023**, *145*, 16090–16097. [CrossRef] [PubMed]
40. Ong, A.; Teo, J.Y.Q.; Feng, Z.; Tan, T.T.Y.; Lim, J.Y.C. Organocatalytic Aerobic Oxidative Degradation of Polystyrene to Aromatic Acids. *ACS Sust. Chem. Eng.* **2023**, *11*, 12514–12522. [CrossRef]

41. Cai, N.; Li, X.; Xia, S.; Sun, L.; Hu, J.; Bartocci, P.; Fantozzi, F.; Williams, P.T.; Yang, H.; Chen, H. Pyrolysis-catalysis of different waste plastics over Fe/Al_2O_3 catalyst: High-value hydrogen, liquid fuels, carbon nanotubes and possible reaction mechanisms. *Energy Convers. Manag.* **2021**, *229*, 113794. [CrossRef]
42. Soares, C.T.d.M.; Ek, M.; Östmark, E.; Gällstedt, M.; Karlsson, S. Recycling of multi-material multilayer plastic packaging: Current trends and future scenarios. *Resour. Conserv. Recycl.* **2022**, *176*, 105905. [CrossRef]
43. Huang, P.; Pitcher, J.; Mushing, A.; Lourenço, F.; Shaver, M.P. Chemical recycling of multi-materials from glycol-modified poly(ethylene terephthalate). *Resour. Conserv. Recycl.* **2023**, *190*, 106854. [CrossRef]
44. Tito, E.; dos Passos, J.S.; Bensaid, S.; Pirone, R.; Biller, P. Multilayer plastic film chemical recycling via sequential hydrothermal liquefaction. *Resour. Conserv. Recycl.* **2023**, *197*, 107067. [CrossRef]
45. Samorì, C.; Pitacco, W.; Vagnoni, M.; Catelli, E.; Colloricchio, T.; Gualandi, C.; Mantovani, L.; Mezzi, A.; Sciutto, G.; Galletti, P. Recycling of multilayer packaging waste with sustainable solvents. *Resour. Conserv. Recycl.* **2023**, *190*, 106832. [CrossRef]
46. Vagnoni, M.; Pitacco, W.; Arpaia, V.; Catelli, E.; Gualandi, C.; Mastroddi, R.; Mezzi, A.; Samorì, C.; Sciutto, G.; Tagliavini, E.; et al. Recycling of multilayer packaging waste with switchable anionic surfactants. *Resour. Conserv. Recycl.* **2023**, *198*, 107141. [CrossRef]
47. Belyamani, I.; Maris, J.; Bourdon, S.; Brossard, J.-M.; Cauret, L.; Fontaine, L.; Montembault, V. Toward recycling "unsortable" post-consumer WEEE stream: Characterization and impact of electron beam irradiation on mechanical properties. *J. Clean. Prod.* **2021**, *294*, 126300. [CrossRef]
48. Thiounn, T.; Karunarathna, M.S.; Lauer, M.K.; Tennyson, A.G.; Smith, R.C. Detoxification of bisphenol A via sulfur-mediated carbon–carbon σ-bond scission. *RSC Sustain.* **2023**, *1*, 535–542. [CrossRef]
49. Maladeniya, C.P.; Tennyson, A.G.; Smith, R.C. Single-stage chemical recycling of plastic waste to yield durable composites via a tandem transesterification-thiocracking process. *J. Polym. Sci.* **2023**, *61*, 787–793. [CrossRef]
50. Wijeyatunga, S.K.; Derr, K.M.; Maladeniya, C.P.; Sauceda-Oloño, P.Y.; Tennyson, A.G.; Smith, R.C. Upcycling waste PMMA to durable composites via a transesterification-inverse vulcanization process. *J. Polym. Sci.* **2023**, *62*, 554–563. [CrossRef]
51. Derr, K.M.; Smith, R.C. One-Pot Method for Upcycling Polycarbonate Waste to Yield High-Strength, BPA-Free Composites. *J. Polym. Sci.* **2023**, *62*, 1115–1122. [CrossRef]
52. Zhang, X.; Tang, Y.; Qu, S.; Da, J.; Hao, Z. H_2S-Selective Catalytic Oxidation: Catalysts and Processes. *ACS Catal.* **2015**, *5*, 1053–1067. [CrossRef]
53. Demirbas, A.; Alidrisi, H.; Balubaid, M.A. API Gravity, Sulfur Content, and Desulfurization of Crude Oil. *Pet. Sci. Technol.* **2015**, *33*, 93–101. [CrossRef]
54. Wolfs, J.; Ribca, I.; Meier, M.A.R.; Johansson, M. Polythionourethane Thermoset Synthesis via Activation of Elemental Sulfur in an Efficient Multicomponent Reaction Approach. *ACS Sust. Chem. Eng.* **2023**, *11*, 3952–3962. [CrossRef]
55. Conen, P.; Nickisch, R.; Meier, M.A.R. Synthesis of highly substituted alkenes by sulfur-mediated olefination of N-tosylhydrazones. *Commun. Chem.* **2023**, *6*, 255. [CrossRef]
56. Nickisch, R.; Conen, P.; Gabrielsen, S.M.; Meier, M.A.R. A more sustainable isothiocyanate synthesis by amine catalyzed sulfurization of isocyanides with elemental sulfur. *RSC Adv.* **2021**, *11*, 3134–3142. [CrossRef]
57. Zhang, Y.; Glass, R.S.; Char, K.; Pyun, J. Recent advances in the polymerization of elemental sulphur, inverse vulcanization and methods to obtain functional Chalcogenide Hybrid Inorganic/Organic Polymers (CHIPs). *Polym. Chem.* **2019**, *10*, 4078–4105. [CrossRef]
58. Chalker, J.M.; Worthington, M.J.H.; Lundquist, N.A.; Esdaile, L.J. Synthesis and Applications of Polymers Made by Inverse Vulcanization. *Top. Curr. Chem.* **2019**, *377*, 16. [CrossRef]
59. Abbasi, A.; Nasef, M.M.; Yahya, W.Z.N. Sulfur-based polymers by inverse vulcanization: A novel path to foster green chemistry. *Green Mater.* **2020**, *8*, 172–180.
60. Wagenfeld, J.-G.; Al-Ali, K.; Almheiri, S.; Slavens, A.F.; Calvet, N. Sustainable applications utilizing sulfur, a by-product from oil and gas industry: A state-of-the-art review. *Waste Manag.* **2019**, *95*, 78–89. [CrossRef] [PubMed]
61. Abbasi, A.; Nasef, M.M.; Yahya, W.Z.N. Copolymerization of vegetable oils and bio-based monomers with elemental sulfur: A new promising route for bio-based polymers. *Sust. Chem. Pharm.* **2019**, *13*, 100158. [CrossRef]
62. Lee, T.; Dirlam, P.T.; Njardarson, J.T.; Glass, R.S.; Pyun, J. Polymerizations with Elemental Sulfur: From Petroleum Refining to Polymeric Materials. *J. Am. Chem. Soc.* **2022**, *144*, 5–22. [CrossRef]
63. Griebel, J.J.; Glass, R.S.; Char, K.; Pyun, J. Polymerizations with elemental sulfur: A novel route to high sulfur content polymers for sustainability, energy and defense. *Prog. Polym. Sci.* **2016**, *58*, 90–125. [CrossRef]
64. Lim, J.; Pyun, J.; Char, K. Recent Approaches for the Direct Use of Elemental Sulfur in the Synthesis and Processing of Advanced Materials. *Angew. Chem. Int. Ed.* **2015**, *54*, 3249–3258. [CrossRef]
65. Chung, W.J.; Griebel, J.J.; Kim, E.T.; Yoon, H.; Simmonds, A.G.; Ji, H.J.; Dirlam, P.T.; Glass, R.S.; Wie, J.J.; Nguyen, N.A.; et al. The use of elemental sulfur as an alternative feedstock for polymeric materials. *Nat. Chem.* **2013**, *5*, 518–524. [CrossRef]
66. Gupta, A.; Worthington, M.J.H.; Patel, H.D.; Johnston, M.R.; Puri, M.; Chalker, J.M. Reaction of Sulfur and Sustainable Algae Oil for Polymer Synthesis and Enrichment of Saturated Triglycerides. *ACS Sustain. Chem. Eng.* **2022**, *10*, 9022–9028. [CrossRef]
67. Worthington, M.J.H.; Kucera, R.L.; Chalker, J.M. Green chemistry and polymers made from sulfur. *Green Chem.* **2017**, *19*, 2748–2761. [CrossRef]

68. Bu Najmah, I.; Lundquist, N.A.; Stanfield, M.K.; Stojcevski, F.; Campbell, J.A.; Esdaile, L.J.; Gibson, C.T.; Lewis, D.A.; Henderson, L.C.; Hasell, T.; et al. Insulating Composites Made from Sulfur, Canola Oil, and Wool**. *ChemSusChem* **2021**, *14*, 2352–2359. [CrossRef]
69. Eder, M.L.; Call, C.B.; Jenkins, C.L. Utilizing Reclaimed Petroleum Waste to Synthesize Water-Soluble Polysulfides for Selective Heavy Metal Binding and Detection. *ACS Appl. Polym. Mater.* **2022**, *4*, 1110–1116. [CrossRef]
70. Gomez, I.; Mecerreyes, D.; Blazquez, J.A.; Leonet, O.; Ben Youcef, H.; Li, C.; Gómez-Cámer, J.L.; Bondarchuk, O.; Rodriguez-Martinez, L. Inverse vulcanization of sulfur with divinylbenzene: Stable and easy processable cathode material for lithium-sulfur batteries. *J. Power Sources* **2016**, *329*, 72–78. [CrossRef]
71. Gomez, I.; Leonet, O.; Blazquez, J.A.; Mecerreyes, D. Inverse Vulcanization of Sulfur using Natural Dienes as Sustainable Materials for Lithium–Sulfur Batteries. *ChemSusChem* **2016**, *9*, 3419–3425. [CrossRef]
72. Griebel, J.J.; Nguyen, N.A.; Namnabat, S.; Anderson, L.E.; Glass, R.S.; Norwood, R.A.; Mackay, M.E.; Char, K.; Pyun, J. Dynamic Covalent Polymers via Inverse Vulcanization of Elemental Sulfur for Healable Infrared Optical Materials. *ACS Macro Lett.* **2015**, *4*, 862–866. [CrossRef]
73. Lundquist, N.A.; Tikoalu, A.D.; Worthington, M.J.H.; Shapter, R.; Tonkin, S.J.; Stojcevski, F.; Mann, M.; Gibson, C.T.; Gascooke, J.R.; Karton, A.; et al. Reactive Compression Molding Post-Inverse Vulcanization: A Method to Assemble, Recycle, and Repurpose Sulfur Polymers and Composites. *Chem. A Eur. J.* **2020**, *26*, 10035–10044. [CrossRef]
74. Yan, P.; Zhao, W.; Tonkin, S.J.; Chalker, J.M.; Schiller, T.L.; Hasell, T. Stretchable and Durable Inverse Vulcanized Polymers with Chemical and Thermal Recycling. *Chem. Mater.* **2022**, *34*, 1167–1178. [CrossRef]
75. Müller, F.G.; Lisboa, L.S.; Chalker, J.M. Inverse Vulcanized Polymers for Sustainable Metal Remediation. *Adv. Sustain. Syst.* **2023**, *7*, 2300010. [CrossRef]
76. Chalker, J.M.; Mann, M.; Worthington, M.J.H.; Esdaile, L.J. Polymers Made by Inverse Vulcanization for Use as Mercury Sorbents. *Org. Mater.* **2021**, *3*, 362–373. [CrossRef]
77. Zhang, B.; Gao, H.; Yan, P.; Petcher, S.; Hasell, T. Inverse vulcanization below the melting point of sulfur. *Mater. Chem. Front.* **2020**, *4*, 669–675. [CrossRef]
78. Smith, J.A.; Mulhall, R.; Goodman, S.; Fleming, G.; Allison, H.; Raval, R.; Hasell, T. Investigating the Antibacterial Properties of Inverse Vulcanized Sulfur Polymers. *ACS Omega* **2020**, *5*, 5229–5234. [CrossRef]
79. Westerman, C.R.; Jenkins, C.L. Dynamic Sulfur Bonds Initiate Polymerization of Vinyl and Allyl Ethers at Mild Temperatures. *Macromolecules* **2018**, *51*, 7233–7238. [CrossRef]
80. Orme, K.; Fistrovich, A.H.; Jenkins, C.L. Tailoring Polysulfide Properties through Variations of Inverse Vulcanization. *Macromolecules* **2020**, *53*, 9353–9361. [CrossRef]
81. Westerman, C.R.; Walker, P.M.; Jenkins, C.L.; Westerman, C.R.; Walker, P.M. Synthesis of Terpolymers at Mild Temperatures Using Dynamic Sulfur Bonds in Poly(S-Divinylbenzene). *JoVE* **2019**, e59620. [CrossRef]
82. Herrera, C.; Ysinga, K.J.; Jenkins, C.L. Polysulfides Synthesized from Renewable Garlic Components and Repurposed Sulfur Form Environmentally Friendly Adhesives. *ACS Appl. Mater. Interfaces* **2019**, *11*, 35312–35318. [CrossRef]
83. Davis, A.E.; Sayer, K.B.; Jenkins, C.L. A comparison of adhesive polysulfides initiated by garlic essential oil and elemental sulfur to create recyclable adhesives. *Polym. Chem.* **2022**, *13*, 4634–4640. [CrossRef]
84. Sayer, K.B.; Miller, V.L.; Merrill, Z.; Davis, A.E.; Jenkins, C.L. Allyl sulfides in garlic oil initiate the formation of renewable adhesives. *Polym. Chem.* **2023**, *14*, 3091–3098. [CrossRef]
85. Duarte, M.E.; Huber, B.; Theato, P.; Mutlu, H. The unrevealed potential of elemental sulfur for the synthesis of high sulfur content bio-based aliphatic polyesters. *Polym. Chem.* **2020**, *11*, 241–248. [CrossRef]
86. Diez, S.; Hoefling, A.; Theato, P.; Pauer, W. Mechanical and Electrical Properties of Sulfur-Containing Polymeric Materials Prepared via Inverse Vulcanization. *Polymers* **2017**, *9*, 59. [CrossRef] [PubMed]
87. Mutlu, H.; Ceper, E.B.; Li, X.; Yang, J.; Dong, W.; Ozmen, M.M.; Theato, P. Sulfur Chemistry in Polymer and Materials Science. *Macromol. Rapid Commun.* **2019**, *40*, 1800650. [CrossRef]
88. Gomez, I.; De Anastro, A.F.; Leonet, O.; Blazquez, J.A.; Grande, H.-J.; Pyun, J.; Mecerreyes, D. Sulfur Polymers Meet Poly(ionic liquid)s: Bringing New Properties to Both Polymer Families. *Macromol. Rapid Commun.* **2018**, *39*, 1800529. [CrossRef]
89. Gomez, I.; Leonet, O.; Alberto Blazquez, J.; Grande, H.-J.; Mecerreyes, D. Poly(anthraquinonyl sulfides): High Capacity Redox Polymers for Energy Storage. *ACS Macro Lett.* **2018**, *7*, 419–424. [CrossRef] [PubMed]
90. Karunarathna, M.S.; Lauer, M.K.; Tennyson, A.G.; Smith, R.C. Copolymerization of an aryl halide and elemental sulfur as a route to high sulfur content materials. *Polym. Chem.* **2020**, *11*, 1621–1628. [CrossRef]
91. Lopez, C.V.; Maladeniya, C.P.; Smith, R.C. Lithium-Sulfur Batteries: Advances and Trends. *Electrochem* **2020**, *1*, 226–259. [CrossRef]
92. Maladeniya, C.P.; Karunarathna, M.S.; Lauer, M.K.; Lopez, C.V.; Thiounn, T.; Smith, R.C. A role for terpenoid cyclization in the atom economical polymerization of terpenoids with sulfur to yield durable composites. *Mater. Adv.* **2020**, *1*, 1665–1674. [CrossRef]
93. Smith, A.D.; Tennyson, A.G.; Smith, R.C. Sulfur-Containing Polymers Prepared from Fatty Acid-Derived Monomers: Application of Atom-Economical Thiol-ene/Thiol-yne Click Reactions and Inverse Vulcanization Strategies. *Sustain. Chem.* **2020**, *1*, 209–237. [CrossRef]
94. Karunarathna, M.S.; Lauer, M.K.; Smith, R.C. Facile route to an organosulfur composite from biomass-derived guaiacol and waste sulfur. *J. Mater. Chem. A* **2020**, *8*, 20318–20322. [CrossRef]

95. Bear, J.C.; Peveler, W.J.; McNaughter, P.D.; Parkin, I.P.; O'Brien, P.; Dunnill, C.W. Nanoparticle-sulphur "inverse vulcanization" polymer composites. *Chem. Commun.* **2015**, *51*, 10467–10470. [CrossRef]
96. Glass, R.S.; Char, K.; Pyun, J. From waste to valuable plastics-Discovery of new paradigms from well-studied systems with elemental sulfur. *Phosphorus Sulfur Silicon Relat. Elem.* **2017**, *192*, 157–161. [CrossRef]
97. Gwon, S.; Jeong, Y.; Oh, J.E.; Shin, M. Sustainable sulfur composites with enhanced strength and lightweightness using waste rubber and fly ash. *Constr. Build. Mater.* **2017**, *135*, 650–664. [CrossRef]
98. Arslan, M.; Kiskan, B.; Cengiz, E.C.; Demir-Cakan, R.; Yagci, Y. Inverse vulcanization of bismaleimide and divinylbenzene by elemental sulfur for lithium sulfur batteries. *Eur. Polym. J.* **2016**, *80*, 70–77. [CrossRef]
99. Boyd, D.A. Sulfur and Its Role in Modern Materials Science. *Angew. Chem. Int. Ed.* **2016**, *55*, 15486–15502. [CrossRef] [PubMed]
100. Cho, W.; Hwang, J.; Lee, S.Y.; Park, J.; Han, N.; Lee, C.H.; Kang, S.-W.; Urbas, A.; Kim, J.O.; Ku, Z.; et al. Highly Sensitive and Cost-Effective Polymeric-Sulfur-Based Mid-Wavelength Infrared Linear Polarizers with Tailored Fabry-Perot Resonance. *Adv. Mater.* **2023**, *35*, 2209377. [CrossRef]
101. Ghosh, A.; Shukla, S.; Khosla, G.S.; Lochab, B.; Mitra, S. Sustainable Sulfur-rich Copolymer/Graphene Composite as Lithium-Sulfur Battery Cathode with Excellent Electrochemical Performance. *Sci. Rep.* **2016**, *6*, 25207. [CrossRef] [PubMed]
102. Mann, M.; Kruger, J.E.; Andari, F.; McErlean, J.; Gascooke, J.R.; Smith, J.A.; Worthington, M.J.H.; McKinley, C.C.C.; Campbell, J.A.; Lewis, D.A.; et al. Sulfur polymer composites as controlled-release fertilizers. *Org. Biomol. Chem.* **2019**, *17*, 1929–1936. [CrossRef]
103. Mohamed, A.-M.O.; El Gamal, M. Hydro-mechanical behavior of a newly developed sulfur polymer concrete. *Cem. Concr. Compos.* **2009**, *31*, 186–194. [CrossRef]
104. Rappold, T.A.; Lackner, K.S. Large scale disposal of waste sulfur: From sulfide fuels to sulfate sequestration. *Energy* **2010**, *35*, 1368–1380. [CrossRef]
105. Stojcevski, F.; Stanfield, M.K.; Hayne, D.J.; Mann, M.; Lundquist, N.A.; Chalker, J.M.; Henderson, L.C. Inverse Vulcanisation of canola oil as a route to recyclable chopped carbon fibre composites. *Sustain. Mater. Technol.* **2022**, *32*, e00400. [CrossRef]
106. Sun, Y.; Yang, C.; Fu, Y.; Guo, T.; Yan, G.; Hu, J. Sulfur-containing adsorbent made by inverse vulcanization of sulfur/oleylamine/potato starch for efficient removal of Hg(II) ions. *J. Environ. Chem. Eng.* **2023**, *11*, 109806. [CrossRef]
107. Wongsirathat, C.; Chavalparit, O. Utilization of sulfur waste from petroleum refinery for sulfur concrete. *Adv. Mater. Res.* **2014**, *856*, 113–117. [CrossRef]
108. Zhang, B.; Petcher, S.; Dop, R.A.; Yan, P.; Zhao, W.; Wang, H.; Dodd, L.J.; McDonald, T.O.; Hasell, T. Inverse vulcanised sulfur polymer nanoparticles prepared by antisolvent precipitation. *J. Mater. Chem. A* **2022**, *10*, 13704–13710. [CrossRef]
109. Scheiger, J.M.; Direksilp, C.; Falkenstein, P.; Welle, A.; Koenig, M.; Heissler, S.; Matysik, J.; Levkin, P.A.; Theato, P. Inverse Vulcanization of Styrylethyltrimethoxysilane-Coated Surfaces, Particles, and Crosslinked Materials. *Angew. Chem. Int. Ed.* **2020**, *59*, 18639–18645. [CrossRef]
110. Griebel, J.J.; Nguyen, N.A.; Astashkin, A.V.; Glass, R.S.; MacKay, M.E.; Char, K.; Pyun, J. Preparation of Dynamic Covalent Polymers via Inverse Vulcanization of Elemental Sulfur. *ACS Macro Lett.* **2014**, *3*, 1258–1261. [CrossRef]
111. Akay, S.; Kayan, B.; Kalderis, D.; Arslan, M.; Yagci, Y.; Kiskan, B. Poly(benzoxazine-co-sulfur): An efficient sorbent for mercury removal from aqueous solution. *J. Appl. Polym. Sci.* **2017**, *134*, 45306. [CrossRef]
112. Ali Ghazi, Z.; Zhu, L.; Wang, H.; Naeem, A.; Khattak, A.M.; Liang, B.; Ali Khan, N.; Wei, Z.; Li, L.; Tang, Z. Efficient Polysulfide Chemisorption in Covalent Organic Frameworks for High-Performance Lithium-Sulfur Batteries. *Adv. Energy Mater.* **2016**, *6*, 1601250. [CrossRef]
113. Arslan, M.; Kiskan, B.; Yagci, Y. Recycling and Self-Healing of Polybenzoxazines with Dynamic Sulfide Linkages. *Sci. Rep.* **2017**, *7*, 5207. [CrossRef]
114. Berk, H.; Kaya, M.; Topcuoglu, M.; Turkten, N.; Karatas, Y.; Cihaner, A. Synthesis, characterization and application of high sulfur content polymeric materials from fatty acids. *React. Funct. Polym.* **2023**, *187*, 105581. [CrossRef]
115. Bhargav, A.; Chang, C.-H.; Fu, Y.; Manthiram, A. Rationally Designed High-Sulfur-Content Polymeric Cathode Material for Lithium-Sulfur Batteries. *ACS Appl. Mater. Interfaces* **2019**, *11*, 6136–6142. [CrossRef] [PubMed]
116. Boyd, D.A.; Nguyen, V.Q.; McClain, C.C.; Kung, F.H.; Baker, C.C.; Myers, J.D.; Hunt, M.P.; Kim, W.; Sanghera, J.S. Optical Properties of a Sulfur-Rich Organically Modified Chalcogenide Polymer Synthesized via Inverse Vulcanization and Containing an Organometallic Comonomer. *ACS Macro Lett.* **2019**, *8*, 113–116. [CrossRef]
117. Ding, N.; Lum, Y.; Chen, S.; Chien, S.W.; Hor, T.S.A.; Liu, Z.; Zong, Y. Sulfur-carbon yolk-shell particle based 3D interconnected nanostructures as cathodes for rechargeable lithium-sulfur batteries. *J. Mater. Chem. A* **2015**, *3*, 1853–1857. [CrossRef]
118. Dop, R.A.; Neill, D.R.; Hasell, T. Sulfur-Polymer Nanoparticles: Preparation and Antibacterial Activity. *ACS Appl. Mater. Interfaces* **2023**, *15*, 20822–20832. [CrossRef]
119. Franz, B.; Lichtenberg, H.; Hormes, J.; Modrow, H.; Dahl, C.; Prange, A. Utilization of solid elemental sulfur by the phototrophic purple sulfur bacterium *Allochromatium vinosum*: A sulfur K-edge X-ray absorption spectroscopy study. *Microbiology* **2007**, *153*, 1268–1274. [CrossRef]
120. Gwon, S.; Ahn, E.; Shin, M. Self-healing of modified sulfur composites with calcium sulfoaluminate cement and superabsorbent polymer. *Compos. Part B Eng.* **2019**, *162*, 469–483. [CrossRef]
121. Key, J.; Feng, Y.; Shen, J.; Wang, P.; Wang, H.; Liang, H.; Wang, R.; Ji, S. A highly crosslinked and conductive sulfur-rich copolymer with grafted polyaniline for stable cycling lithium-sulfur batteries. *J. Electrochem. Soc.* **2020**, *167*, 20530. [CrossRef]

122. Lundquist, N.A.; Yin, Y.; Mann, M.; Tonkin, S.J.; Slattery, A.D.; Andersson, G.G.; Gibson, C.T.; Chalker, J.M. Magnetic responsive composites made from a sulfur-rich polymer. *Polym. Chem.* **2022**, *13*, 5659–5665. [CrossRef]
123. Lopez, C.V.; Smith, R.C. Chemical Recycling of Poly(ethylene terephthalate) via Sequential Glycolysis, Oleoyl Chloride Esterification and Vulcanization to yield Durable Composites. *Mater. Adv.* **2023**, *4*, 2785–2793. [CrossRef]
124. Derr, K.M.; Lopez, C.V.; Maladeniya, C.P.; Tennyson, A.G.; Smith, R.C. Transesterification-vulcanization route to durable composites from post-consumer poly(ethylene terephthalate), terpenoids, and industrial waste sulfur. *J. Polym. Sci.* **2023**, *61*, 3075–3086. [CrossRef]
125. Lopez, C.V.; Smith, R.C. Composites produced from Waste Plastic with Agricultural and Energy Sector by-Products. *J. Appl. Polym. Sci.* **2023**, *141*, e54828. [CrossRef]
126. Karunarathna, M.S.; Maladeniya, C.P.; Lauer, M.K.; Tennyson, A.G.; Smith, R.C. Durable Composites by Vulcanization of Oleyl-Esterified Lignin. *RSC Adv.* **2023**, *13*, 3234–3240. [CrossRef]
127. Karunarathna, M.S.; Tennyson, A.G.; Smith, R.C. Facile new approach to high sulfur-content materials and preparation of sulfur-lignin copolymers. *J. Mater. Chem. A* **2020**, *8*, 548–553. [CrossRef]
128. Karunarathna, M.S.; Lauer, M.K.; Thiounn, T.; Smith, R.C.; Tennyson, A.G. Valorization of waste to yield recyclable composites of elemental sulfur and lignin. *J. Mater. Chem. A* **2019**, *7*, 15683–15690. [CrossRef]
129. Lauer, M.K.; Estrada-Mendoza, T.A.; McMillen, C.D.; Chumanov, G.; Tennyson, A.G.; Smith, R.C. Durable Cellulose-Sulfur Composites Derived from Agricultural and Petrochemical Waste. *Adv. Sustain. Syst.* **2019**, *3*, 1900062. [CrossRef]
130. Lauer, M.K.; Tennyson, A.G.; Smith, R.C. Thermomorphological and mechanical properties of vulcanized octenyl succinate/terpenoid-derivatized corn starch composites. *Mater. Adv.* **2022**, *3*, 4186–4193. [CrossRef]
131. Lauer, M.K.; Tennyson, A.G.; Smith, R.C. Inverse vulcanization of octenyl succinate-modified corn starch as a route to biopolymer-sulfur composites. *Mater. Adv.* **2021**, *2*, 2391–2397. [CrossRef]
132. Lauer, M.K.; Karunarathna, M.S.; Tennyson, A.G.; Smith, R.C. Recyclable, sustainable, and stronger than portland cement: A composite from unseparated biomass and fossil fuel waste. *Mater. Adv.* **2020**, *1*, 590–594. [CrossRef]
133. Lauer, M.K.; Karunarathna, M.S.; Tennyson, A.G.; Smith, R.C. Robust, remeltable and remarkably simple to prepare biomass-sulfur composites. *Mater. Adv.* **2020**, *1*, 2271–2278. [CrossRef]
134. Insights, S.M. Peanut Butter—Worldwide. Available online: https://www-statista-com.libproxy.clemson.edu/outlook/cmo/food/spreads-sweeteners/spreads/peanut-butter/worldwide (accessed on 4 December 2023).
135. Sheldon, R.A. The E Factor: Fifteen years on. *Green Chem.* **2007**, *9*, 1273–1283. [CrossRef]
136. Dale, J.J.; Stanley, J.; Dop, R.A.; Chronowska-Bojczuk, G.; Fielding, A.J.; Neill, D.R.; Hasell, T. Exploring Inverse Vulcanisation Mechanisms from the Perspective of Dark Sulfur. *Eur. Polym. J.* **2023**, *195*, 112198. [CrossRef]
137. Bao, J.; Martin, K.P.; Cho, E.; Kang, K.-S.; Glass, R.S.; Coropceanu, V.; Bredas, J.-L.; Parker, W.O.N., Jr.; Njardarson, J.T.; Pyun, J. On the Mechanism of the Inverse Vulcanization of Elemental Sulfur: Structural Characterization of Poly(sulfur-random-(1,3-diisopropenylbenzene)). *J. Am. Chem. Soc.* **2023**, *145*, 12386–12397. [CrossRef]
138. Kang, K.-S.; Iyer, K.A.; Pyun, J. On the Fundamental Polymer Chemistry of Inverse Vulcanization for Statistical and Segmented Copolymers from Elemental Sulfur. *Chem. A Eur. J.* **2022**, *28*, e202200115. [CrossRef]
139. Smith, J.A.; Wu, X.; Berry, N.G.; Hasell, T. High sulfur content polymers: The effect of crosslinker structure on inverse vulcanization. *J. Polym. Sci. Part A Polym. Chem.* **2018**, *56*, 1777–1781. [CrossRef]
140. Parker, D.J.; Chong, S.T.; Hasell, T. Sustainable inverse-vulcanised sulfur polymers. *RSC Adv.* **2018**, *8*, 27892–27899. [CrossRef]
141. Dunn, J.; Jenkins, C.L. Making light of inverse vulcanization. *Nat. Synth.* **2022**, *1*, 835–836. [CrossRef]
142. Lopez, C.V.; Karunarathna, M.S.; Lauer, M.K.; Maladeniya, C.P.; Thiounn, T.; Ackley, E.D.; Smith, R.C. High Strength, Acid-Resistant Composites from Canola, Sunflower, or Linseed Oils: Influence of Triglyceride Unsaturation on Material Properties. *J. Poly. Sci.* **2020**, *58*, 2259–2266. [CrossRef]
143. Lauer, M.K.; Tennyson, A.G.; Smith, R.C. Green Synthesis of Thermoplastic Composites from a Terpenoid-Cellulose Ester. *ACS Appl. Polym. Mater.* **2020**, *2*, 3761–3765. [CrossRef]
144. Lopez, C.V.; Smith, A.D.; Smith, R.C. High strength composites from low-value animal coproducts and industrial waste sulfur. *RSC Adv.* **2022**, *12*, 1535–1542. [CrossRef]
145. Guinati, B.G.S.; Sauceda Oloño, P.Y.; Kapuge Dona, N.L.; Derr, K.M.; Wijeyatunga, S.K.; Tennyson, A.G.; Smith, R.C. Upcycling mixed-material waste with elemental sulfur: Applications to plant oil, unseparated biomass, and raw post-consumer food waste. *RSC Sustain.* **2024**, *2*, 1819–1827. [CrossRef]
146. Dale, J.J.; Petcher, S.; Hasell, T. Dark Sulfur: Quantifying Unpolymerized Sulfur in Inverse Vulcanized Polymers. *ACS Appl. Polym. Mater.* **2022**, *4*, 3169–3173. [CrossRef]
147. Kulkarni, P.; Ravekar, V.; Rama Rao, P.; Waigokar, S.; Hingankar, S. Recycling of waste HDPE and PP plastic in preparation of plastic brick and its mechanical properties. *Clean. Mater.* **2022**, *5*, 100113. [CrossRef]
148. Mohammed, A.A.; Mohammed, I.I.; Mohammed, S.A. Some properties of concrete with plastic aggregate derived from shredded PVC sheets. *Constr. Build. Mater.* **2019**, *201*, 232–245. [CrossRef]
149. Attanasio, A.; Largo, A.; Alvarez, I.L.; Sonzogni, F.; Balaceanu, L. Sustainable aggregates from secondary materials for innovative lightweight concrete products. *Heron* **2015**, *60*, 5–26.
150. Wu, H.; Liu, Z.; Sun, B.; Yin, J. Experimental investigation on freeze–thaw durability of Portland cement pervious concrete (PCPC). *Constr. Build. Mater.* **2016**, *117*, 63–71. [CrossRef]

151. Phan, T.V.T.; Gallardo, C.; Mane, J. GREEN MOTION: A new and easy to use green chemistry metric from laboratories to industry. *Green Chem.* **2015**, *17*, 2846–2852. [CrossRef]
152. Dormer, A.; Finn, D.P.; Ward, P.; Cullen, J. Carbon footprint analysis in plastics manufacturing. *J. Clean. Prod.* **2013**, *51*, 133–141. [CrossRef]
153. Turner, L.K.; Collins, F.G. Carbon dioxide equivalent (CO_2-e) emissions: A comparison between geopolymer and OPC cement concrete. *Constr. Build. Mater.* **2013**, *43*, 125–130. [CrossRef]
154. Allwood, J.M.; Cullen, J.M.; Milford, R.L. Options for Achieving a 50% Cut in Industrial Carbon Emissions by 2050. *Environ. Sci. Technol.* **2010**, *44*, 1888–1894. [CrossRef]
155. Brogaard, L.K.; Damgaard, A.; Jensen, M.B.; Barlaz, M.; Christensen, T.H. Evaluation of life cycle inventory data for recycling systems. *Resour. Conserv. Recycl.* **2014**, *87*, 30–45. [CrossRef]
156. Mokhtar, A.; Nasooti, M. A decision support tool for cement industry to select energy efficiency measures. *Energy Strategy Rev.* **2020**, *28*, 100458. [CrossRef]
157. Chen, C.; Habert, G.; Bouzidi, Y.; Jullien, A. Environmental impact of cement production: Detail of the different processes and cement plant variability evaluation. *J. Clean. Prod.* **2010**, *18*, 478–485. [CrossRef]
158. Drabczyk, A.; Kudłacik-Kramarczyk, S.; Korniejenko, K.; Figiela, B.; Furtos, G. Review of Geopolymer Nanocomposites: Novel Materials for Sustainable Development. *Materials* **2023**, *16*, 3478. [CrossRef]
159. Furtos, G.; Molnar, L.; Silaghi-Dumitrescu, L.; Pascuta, P.; Korniejenko, K. Mechanical and thermal properties of wood fiber reinforced geopolymer composites. *J. Nat. Fibers* **2022**, *19*, 6676–6691. [CrossRef]
160. Furtos, G.; Silaghi-Dumitrescu, L.; Pascuta, P.; Sarosi, C.; Korniejenko, K. Mechanical Properties of Wood Fiber Reinforced Geopolymer Composites with Sand Addition. *J. Nat. Fibers* **2021**, *18*, 285–296. [CrossRef]
161. Arena, U.; Ardolino, F. Technical and environmental performances of alternative treatments for challenging plastics waste. *Resour. Conserv. Recycl.* **2022**, *183*, 106379. [CrossRef]
162. Jeswani, H.; Krüger, C.; Russ, M.; Horlacher, M.; Antony, F.; Hann, S.; Azapagic, A. Life cycle environmental impacts of chemical recycling via pyrolysis of mixed plastic waste in comparison with mechanical recycling and energy recovery. *Science of the Total Environment* **2021**, *769*, 144483. [CrossRef]
163. Lewis, G.N.; Randall, M. The Heat Content Of the Various Forms of Sulfur. *J. Am. Chem. Soc.* **1911**, *33*, 476–488. [CrossRef]
164. McCarty, J.A.; Sandefur, H.N.; Matlock, M.; Thoma, G.; Kim, D. Life cycle assessment of greenhouse gas emissions associated with production and consumption of peanut butter in the US. *Trans. ASABE* **2014**, *57*, 1741–1750.
165. Passarini, F.; Ciacci, L.; Santini, A.; Vassura, I.; Morselli, L. Auto shredder residue LCA: Implications of ASR composition evolution. *J. Clean. Prod.* **2012**, *23*, 28–36. [CrossRef]
166. Peukert, W. Material properties in fine grinding. *Int. J. Miner. Process.* **2004**, *74*, S3–S17. [CrossRef]
167. Schubert, G.; Bernotat, S. Comminution of non-brittle materials. *Int. J. Miner. Process.* **2004**, *74*, S19–S30. [CrossRef]
168. Tomberlin, K.E.; Venditti, R.; Yao, Y. Life cycle carbon footprint analysis of pulp and paper grades in the united states using production-line-based data and integration. *BioResources* **2020**, *15*, 3899–3914. [CrossRef]
169. Wüstenberg, D.; Kasper, J. Required energy and structural breakdown at the process of dynamic cutting—Comminution of polypropylene and aluminium. *Int. J. Miner. Process.* **2004**, *74*, S417–S424. [CrossRef]
170. Zheng, J.; Suh, S. Strategies to reduce the global carbon footprint of plastics. *Nat. Clim. Chang.* **2019**, *9*, 374–378. [CrossRef]